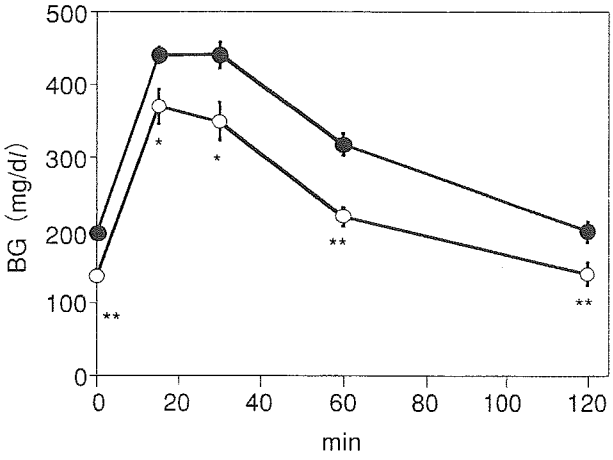

図5　糖負荷試験．肝におけるUCP1発現により，個体レベルでの耐糖能の改善が認められた．（●コントロールマウス，○UCP1発現マウス）

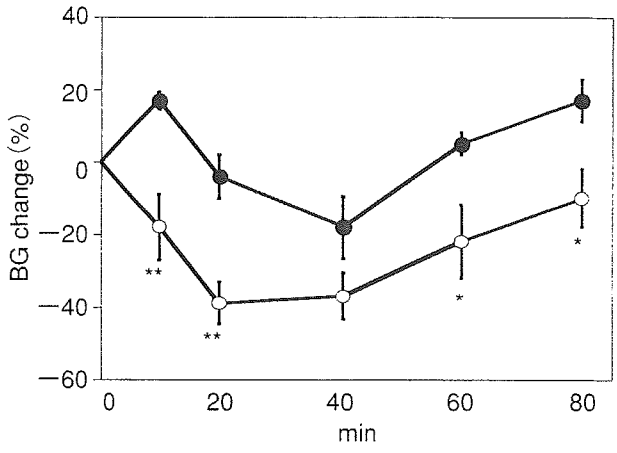

図6　インスリン負荷試験．肝におけるUCP1発現により，個体レベルでのインスリン抵抗性の改善が認められた．（●コントロールマウス，○UCP1発現マウス）

りしているということを示している．これらのメカニズムにより，個体レベルでは，耐糖能（図5）やインスリン感受性の改善（図6）・血中脂質の低下が認められ，メタボリックシンドロームに対する著明な治療効果を認めた．

さらに，興味深いことに，標準餌にて飼育している非肥満・非糖尿病マウスに対しては，肝臓へのUCP1発現にてもエネルギー代謝は亢進せず，体重や耐糖能には影響しないという結果が得られた．その理由として，UCP1がプロトンを輸送する際，脂肪酸が必要である[5]ことが知られていることから，肝臓における異所性UCP1のプロトン輸送活性は肝脂肪などのエネルギー代謝状況により調節される，つまり，肝臓内での異所性UCP1は，エネルギーバランスを感知し，エネルギー過剰状態のときにのみその機能を発揮するセンサーの役割を果たしているという機序が想定される．肝臓へのUCP1遺伝子導入では，余剰カロリーは効果的に消費されるが，必要カロリーの消費については影響を受けにくいというわけで，このことは実際の治療への応用を考えた場合，非常に好ましい結果である[4]．

また，病態発症後の脂肪細胞におけるUCP1遺伝子導入においても，さらに強力な治療効果が認められている．肝臓へのUCP1遺伝子導入と同様に，高脂肪食により肥満・糖尿病を発症させたマウスの副睾丸周囲脂肪組織に，アデノウイルスベクターを用いてUCP1遺伝子導入を行ったところUCP1の発現は局所的・限定的で，全身のエネルギー消費量には増加を認めない程度であったにもかかわらず，肥満・糖尿病の基本病態と考えられるインスリン抵抗性・レプチン抵抗性を改善し，糖尿病や肥満症への著明な治療効果を認めた[6]．これもまた，脂肪組織と遠隔臓器・組織との情報のやり取りを示すものと考えられ，その機構が，肥満・糖尿病の新規治療の有望なターゲットとなりうる．このように，病態発症後の後天的遺伝子導入による急性の治療効果を検討することにより，まだ解明されていない臓器・組織間の相互作用・情報のやりとりを示唆する現象を観察することができる．現在，これらの機構の解明やその調節による肥満・糖尿病に対する創薬を目指して研究を進めている．

おわりに

エネルギー蓄積過剰に基づく病態を改善させるには，エネルギー摂取の抑制あるいはエネ

ネルギー消費の亢進が必要である．個体は一つ一つの臓器が独立して代謝を担っているだけでなく，これらの協調作用によって，全身の恒常性が維持されている．この破綻が，肥満・糖尿病・メタボリックシンドロームなどの代謝性疾患であると考えてよかろう．この病態の基盤として，インスリン抵抗性とレプチン抵抗性が存在するものと考える．しかし，レプチン抵抗性については，その分子機構についても不明であり，摂食調節や臓器・組織間の情報のやり取りの機序も含め，解明すべき問題が数多く残されている．これらの分野の研究が進むことで，生体が個体としての恒常性を保つ根本的な機構の解明につながるものと考えられるのみならず，メタボリックシンドロームに対する画期的な治療法開発につながることを期待したい．

文献

1) Kopecky J, et al : Expression of the mitochondrial uncoupling protein gene from the aP 2 gene promoter prevents genetic obesity. J Clin Invest 96 : 2914-2923, 1995
2) Katagiri H, et al : Overexpression of catalytic subunit p 110 alpha of phosphatidylinositol 3-kinase increases glucose transport activity with translocation of glucose transporters in 3 T 3-L 1 adipocytes. J Biol Chem 271 : 16987-16990, 1996
3) Enerback S, et al : Mice lacking mitochondrial uncoupling protein are cold-sensitive but not obese. Nature, 387 : 90-94, 1997
4) Ishigaki Y, Katagiri H, Yamada T, et al : Dissipating excess energy in the liver is a potential treatment strategy for diabetes associated with obesity. Diabetes 54 : 322-332, 2005
5) Winkler E, Klingenberg M : Effect of fatty acids on H + transport activity of the reconstituted uncoupling protein. J Biol Chem 269 (4) : p. 2508-2515, 1994
6) Yamada T, Katagiri H, Ishigaki Y, et al : submitted

Signals from intra-abdominal fat modulate insulin and leptin sensitivity through different mechanisms: Neuronal involvement in food-intake regulation

Tetsuya Yamada,[1,7] Hideki Katagiri,[2,7,*] Yasushi Ishigaki,[1,7] Takehide Ogihara,[2] Junta Imai,[1,2] Kenji Uno,[1,2] Yutaka Hasegawa,[1,2] Junhong Gao,[1,2] Hisamitsu Ishihara,[1] Akira Niijima,[3] Hiroyuki Mano,[4] Hiroyuki Aburatani,[5] Tomoichiro Asano,[6] and Yoshitomo Oka[1]

[1] Division of Molecular Metabolism and Diabetes
[2] Division of Advanced Therapeutics for Metabolic Diseases, Center for Translational and Advanced Animal Research
Tohoku University Graduate School of Medicine, Sendai 980-8575, Japan
[3] Niigata University School of Medicine, Niigata 951-8150, Japan
[4] Division of Functional Genomics, Jichi Medical School, Kawachi-gun, Tochigi 329-0498, Japan
[5] Research Center for Advanced Science and Technology, University of Tokyo, Tokyo 153-8904, Japan
[6] Department of Physiological Chemistry and Metabolism, University of Tokyo, Tokyo 113-8655, Japan
[7] These authors contributed equally to this work.
*Correspondence: katagiri-tky@umin.ac.jp

Summary

Intra-abdominal fat accumulation is involved in development of the metabolic syndrome, which is associated with insulin and leptin resistance. We show here that ectopic expression of very low levels of uncoupling protein 1 (UCP1) in epididymal fat (Epi) reverses both insulin and leptin resistance. UCP1 expression in Epi improved glucose tolerance and decreased food intake in both diet-induced and genetically obese mouse models. In contrast, UCP1 expression in Epi of leptin-receptor mutant mice did not alter food intake, though it significantly decreased blood glucose and insulin levels. Thus, hypophagia induction requires a leptin signal, while the improved insulin sensitivity appears to be leptin independent. In wild-type mice, local-nerve dissection in the epididymis or pharmacological afferent blockade blunted the decrease in food intake, suggesting that afferent-nerve signals from intra-abdominal fat tissue regulate food intake by modulating hypothalamic leptin sensitivity. These novel signals are potential therapeutic targets for the metabolic syndrome.

Introduction

The explosive increase in obesity has become a major public health concern in most industrialized countries (Flier, 2004; Friedman, 2003). Insulin resistance is a fundamental contributor to the metabolic syndrome associated with type 2 diabetes, hypertension, hyperlipidemia, and atherosclerosis. Major advancements in this field include the discoveries of adipocyte-derived humoral factors, such as leptin (Friedman and Halaas, 1998). Leptin conveys energy-storage information from adipose tissue to the central nervous system, leading to food-intake suppression. However, in patients with ordinary obesity, serum leptin levels are increased in proportion to body fat (Considine et al., 1996), but the responses to leptin are impaired (Heymsfield et al., 1999), which defines a state of leptin resistance. Leptin resistance also contributes to the development of obesity and obesity-related metabolic disorders.

Fat accumulation in intra-abdominal fat tissue is involved in development of the metabolic syndrome (Bjorntorp, 1992; Matsuzawa et al., 1995) associated with insulin and leptin resistance (Friedman, 2003). Therefore, in this study, to examine whether the metabolic changes in intra-abdominal fat tissue affect insulin and leptin resistance as well as systemic glucose metabolism, we attempted to express uncoupling protein 1 (UCP1), which functions to dissipate energy as heat (Klingenberg and Huang, 1999), in epididymal fat tissue (Epi) in mice with obesity and diabetes.

Results and discussion

C57BL/6 mice were subjected to direct injection of the UCP1 adenovirus vector into Epi (UCP1 mice) after the development of diabetes associated with obesity in response to high-fat chow preloading for 4 weeks. Mice given the LacZ adenovirus were used as controls (LacZ mice). Immunoblotting detected adenovirus-mediated UCP1 expression in Epi (see Figure S1A in the Supplemental Data available with this article online), and this expression was restricted to Epi (Fig. S1A). UCP1 expression in Epi was detectable on the first day after adenoviral injection and was increased on day 3 but had fallen to very low levels by day 7 (Figure S1B). However, expression levels were far below those of endogenous protein in BAT: on day 3, approximately 5% per unit weight protein (Figure S1B). UCP1 expression was restricted to very limited portions of the tissue (left panel of Figure 1B). Judging from the intensity of immunostaining, UCP1 expression levels in UCP1-expressing white adipocytes did not reach those in brown adipocytes (right panel of Figure 1B). UCP1-expressing adipocytes were significantly smaller than UCP1-nonexpressing adipocytes in the same tissue (Figure 1C), suggesting enhanced metabolism in the former.

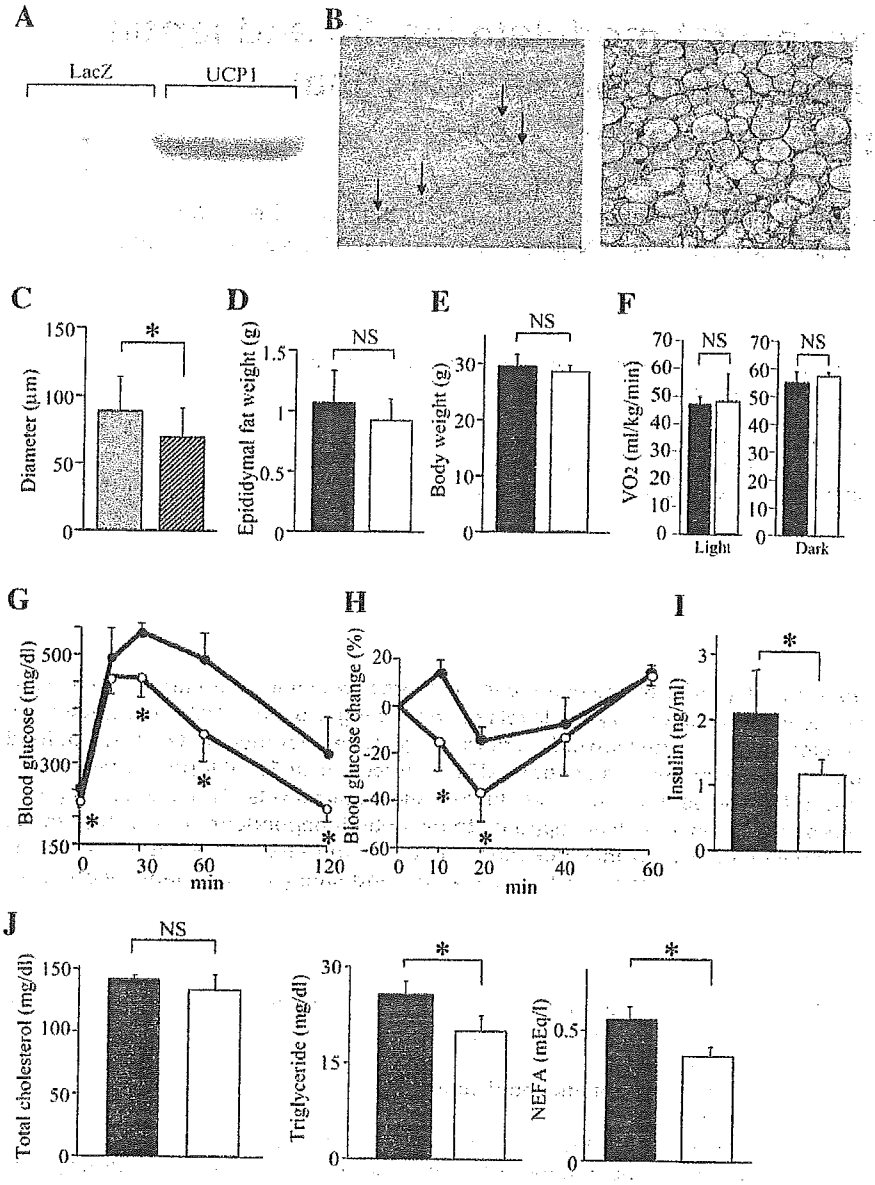

Figure 1. UCP1 expression in Epi improved glucose tolerance and insulin sensitivity

A) Immunoblotting, with anti-UCP1 antibody, of Epi extracts from LacZ and UCP1 mice on day 3 after adenoviral administration.

B) Immunohistochemistry, with anti-UCP1 antibody, of Epi (left panel) and BAT (right panel) sections from a UCP1 mouse on day 3 after adenoviral administration. These two samples were immunostained under the same conditions.

C) Diameters of UCP1-nonexpressing (gray bar) and UCP1-expressing (hatched bar) adipocytes in Epi from UCP1 mice on day 3 after adenoviral administration.

D–J) Epididymal fat weights (**D**), body weights (**E**), resting oxygen consumption during light and dark phase (**F**), and metabolic parameters (**G–J**) of LacZ mice (black bars) and UCP1 mice (white bars) on day 3 after adenoviral administration. Glucose-tolerance (**G**) and insulin-tolerance tests (**H**) were performed on day 3. Data in (**H**) are expressed as percentages of the blood glucose levels immediately before intraperitoneal insulin loading. Serum insulin levels (**I**) and serum lipid parameters ([**J**]; left: total cholesterol, middle: triglyceride, right: free fatty acids) were measured after a 10 hr fast (n = 6 per group). Data are presented as means ± SD (n = 6 per group). *$p < 0.05$ by unpaired t test.

We further confirmed enhanced metabolism by adenoviral UCP1 expression using 3T3-L1 adipocytes. UCP1 expression decreased intracellular ATP concentrations (Figure S1C) and increased levels of peroxisome proliferator-activated receptor γ coactivator (PGC) 1α and cytochrome c expression (Figure S1D). Thus, exogenous UCP1 was functionally active, resulting in increased mitochondrial biosynthesis in adipocytes.

However, neither total Epi weights nor body weights differed between LacZ and UCP1 mice on day 3 after adenoviral administration (Figures 1D and 1E). Oxygen consumption was not affected by UCP1 expression in Epi during either the light or the dark phase (Figure 1F), also reflecting the very limited UCP1 expression. Therefore, to avoid the secondary effects of body-weight change, we analyzed metabolic parameters on day 3. To our surprise, however, even very limited UCP1 expression in Epi resulted in marked changes in metabolic phenotype.

Glucose- and insulin-tolerance tests indicated marked improvements in glucose tolerance and insulin sensitivity (Figures 1G and 1H). Fasting blood glucose (Figure 1G) and insulin (Figure 1I) levels were significantly lower in UCP1 mice, further confirming improved insulin sensitivity. In addition, serum lipid parameters, including triglycerides and free fatty acids (Figure 1J), were also improved with UCP1 expression in Epi. Thus, limited regional expression of UCP1 in Epi markedly improved systemic insulin resistance, resulting in improvement of diabetes and dyslipidemia.

Next, we measured serum adipocytokine levels (Figure 2A). Adiponectin and tumor necrosis factor α levels were not significantly altered. In contrast, serum leptin was markedly decreased, by 46%, with UCP1 expression in Epi. Although intra-abdominal fat-tissue weights were unaltered or only very slightly decreased in UCP1 mice (Figure 1D and Figure S1E),

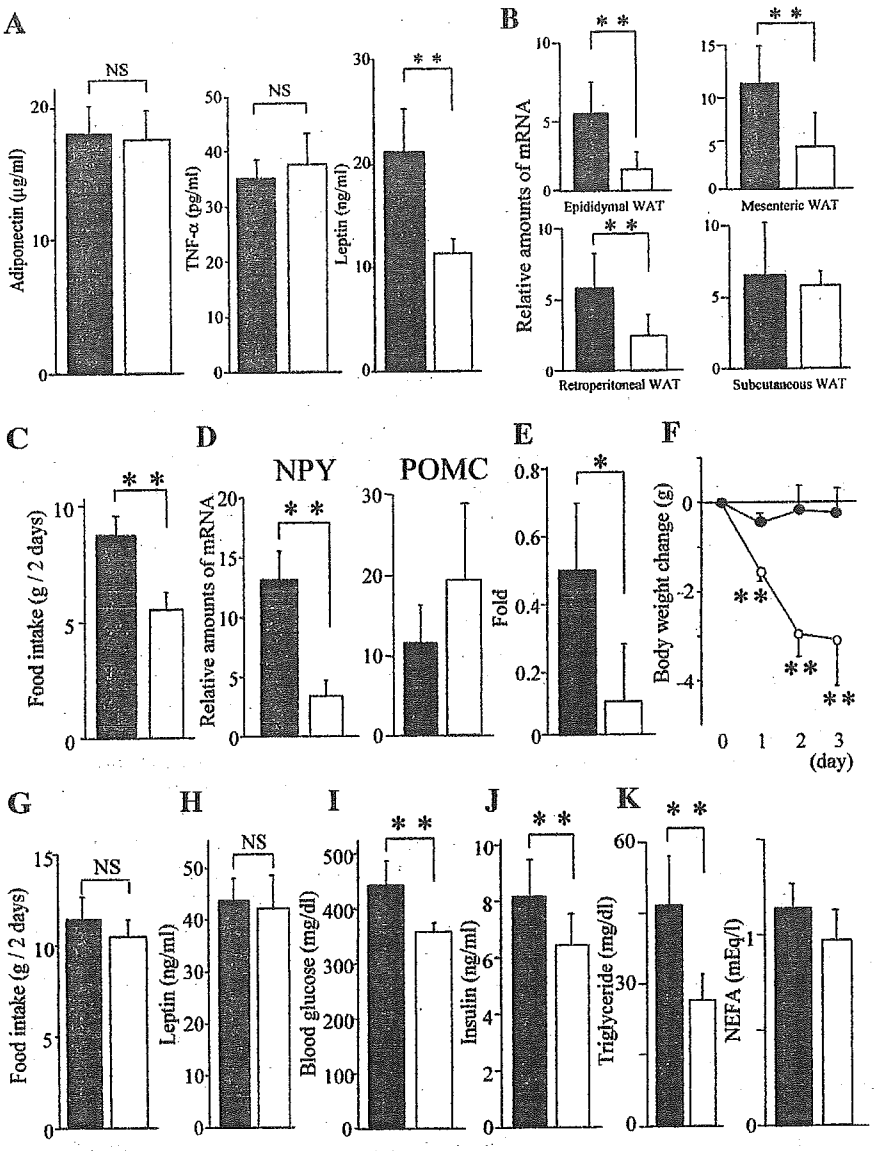

Figure 2. UCP1 expression in Epi improved leptin sensitivity

A–F) LacZ (black bars) or UCP1 (white bars) adenovirus was injected into Epi of mice with dietary obesity.

A) Serum adipocytokine levels (left: adiponectin, middle: TNFα, right: leptin) in LacZ mice and UCP1 mice after a 10 hr fast on day 3 after adenoviral administration.

B) Relative amounts of leptin mRNA in adipose tissues.

C) Total food intakes on days 2 and 3 after adenoviral administration.

D) Relative amounts of neuropeptide Y (left) and proopiomelanocortin (right) mRNA were measured by quantitative RT-PCR using total RNA obtained from the hypothalamus on day 2 after adenoviral administration. Data were corrected with β-actin as the standard (**B** and **D**).

E and F) Leptin-tolerance tests were performed on day 3 after adenoviral administration. Data were expressed as ratios to the food intakes of vehicle-treated mice (**E**). Mice were weighed at 12 hr after each daily injection of leptin or vehicle (**F**).

G–K) LacZ (black bars) or UCP1 (white bars) adenovirus was injected into Epi of db/db mice.

G) Total food intakes on days 2 and 3 after adenoviral administration are presented.

H–K) Blood leptin (**H**), glucose (**I**), and insulin (**J**) levels and serum lipid parameters (**K**; left: triglyceride, right: free fatty acids) of db/db mice were measured after a 10 hr fast. Data are presented as means ± SD (n = 8 per group). *$p < 0.05$; **$p < 0.01$ by unpaired t test.

leptin mRNA expression was markedly decreased in intra-abdominal fat tissues (Figure 2B). Thus, the effects of UCP1 expression in Epi are also exerted in fat tissues other than those injected with the adenovirus. Food intake was significantly suppressed (Figure 2C), indicating that hypothalamic leptin sensitivity was markedly improved despite the lack of significant changes in body weights. Decreased leptin expression in several adipose tissues suggests efferent sympathetic nerve activation, which also supports leptin signal enhancement.

Administration of green fluorescent protein-adenovirus exerted minimal metabolic effects (Figures S1F–S1J). On day 7, when adenoviral UCP1 expression was markedly decreased (Figure S1B), blood glucose, insulin, and leptin levels did not differ between the UCP1 and LacZ mice (Figure S2). In addition, we confirmed the metabolic effects of UCP1 expression in Epi using three other obese models: AKR mice on high-fat chow and KK mice and KK-Ay mice on normal chow. In these three models, similar metabolic impacts were observed with UCP1 adenovirus administration into Epi (Figure S3). Thus, UCP1 expression in Epi exerts acute, beneficial metabolic effects in both diet-induced and genetically obese models.

Increased leptin signals in the hypothalamus induced by UCP1 expression in Epi were further confirmed by changed levels of hypothalamic neuropeptide expression in UCP1 mice on day 3 after adenoviral administration. Real-time RT-PCR revealed adipose UCP1 expression to significantly decrease expression of neuropeptide Y, an orexigenic neuropeptide, while tending to increase that of proopiomelanocortin, a precursor of an anorexigenic neuropeptide, in the hypothalamus (Figure 2D).

To directly test whether leptin sensitivity was improved, we performed leptin-tolerance tests. When leptin was injected intraperitoneally into fasting mice on day 3, leptin-induced food-intake inhibition was far more profound in UCP1 mice than in LacZ mice (Figure 2E). In addition, when leptin was given daily, body weights were significantly decreased (Figure 2F). Thus,

even very limited UCP1 expression in Epi exerts a remote therapeutic effect on hypothalamic leptin resistance, which had already developed in response to preloading with high-fat chow. Transgenic overexpression of UCP1 (Kopecky et al., 1995) and rather minor induction of UCP1 in white adipose tissue (Cederberg et al., 2001; Leonardsson et al., 2004; Tsukiyama-Kohara et al., 2001; Um et al., 2004) result in resistance to high-fat-diet-induced obesity but do not reportedly cause hyperphagia. In this study, however, we expressed UCP1 after the development of obesity and leptin resistance and were thus able to observe acute, beneficial effects, i.e., improved leptin sensitivity, which would be difficult to detect using congenitally UCP1-overexpressing mice.

Increased leptin sensitivity is likely to be involved in the phenotype of UCP1 mice. If this is the case, at least some of the phenotypic features of UCP1 mice would presumably be absent in mice lacking the hypothalamic leptin signal. To test this, UCP1 or LacZ adenovirus was injected into Epi of db/db mice, leptin-receptor Ob-Rb mutants. Food intake (Figure 2G) and serum leptin (Figure 2H) did not differ between LacZ-expressing and UCP1-expressing db/db mice. These findings confirm that the effect of UCP1 expression in Epi on food intake is leptin-signal dependent. On the other hand, UCP1 expression in Epi of db/db mice caused small but significant decreases in blood glucose (Figure 2I), insulin (Figure 2J), and triglyceride (Figure 2K) levels, as well as tending to decrease serum free-fatty-acid levels (Figure 2K). These findings demonstrate that UCP1 expression in Epi improves insulin sensitivity, in part, independently of leptin signaling.

To eliminate the secondary effects of reduced food intake, pair-feeding experiments were performed using C57BL/6 wild-type mice (Figure S4). Pair feeding did not significantly alter the body weights of LacZ mice. Fasting blood glucose did not differ between UCP1 mice and pair-fed LacZ mice, but after glucose loading, blood glucose levels were significantly lower in UCP1 mice. In addition, serum insulin and leptin levels were significantly lower in UCP1 mice than in pair-fed LacZ mice. Taken together with the results obtained using db/db mice, the improved insulin sensitivity induced by UCP1 expression in Epi appears not to be mediated solely by decreased food intake.

The same amounts of recombinant adenovirus encoding UCP1 were directly injected into subcutaneous fat tissues in the flank of C57BL/6 mice with dietary obesity and diabetes. UCP1 expression levels were similar to those obtained by injection into Epi (data not shown). Food intake was significantly decreased by UCP1 expression, as compared with LacZ expression, in subcutaneous fat (Figure 3A), but the effects were much smaller than those produced by UCP1 expression in Epi (Figure 2C). Furthermore, there were no statistically significant decreases in blood glucose (Figure 3B), insulin (Figure 3C), or leptin (Figure 3D) levels. Thus, exogenous UCP1 expression in subcutaneous fat was far less effective in improving insulin and leptin resistance than that in intra-abdominal fat tissue. These findings suggest the anatomical location of the manipulated adipose tissue to be involved in the observed therapeutic effects, which would appear to be important for understanding the metabolic differences between visceral fat-dominant and subcutaneous fat-dominant obesity.

How does the signal (or signals) from intra-abdominal fat tissue exert these remote effects? The importance of anatomical fat-tissue location suggests the involvement of neuronal signaling. The afferent activity from Epi is reportedly transmitted through the nerve bundle, which runs alongside blood vessels supplying Epi, in rats (Niijima, 1998). To study the possible involvement of neuronal signals from Epi, we dissected this nerve bundle in mice with dietary obesity and diabetes. Ten days after bilateral nerve-bundle dissection, adenoviruses were injected into Epi. No significant differences in body weights or Epi weights were observed between sham-operated and nerve-dissected mice (data not shown). While UCP1 adenoviral administration significantly decreased food intake in sham-operated mice, nerve dissection blunted this decrease in food intake such that it was no longer statistically significant (Figure 3E). Similarly, nerve dissection blunted a decrease in hypothalamic NPY mRNA expression, rendering it statistically insignificant (NPY; LacZ versus UCP1: 12.06 ± 6.16 versus 6.39 ± 3.10; $p = 0.15$). These findings suggest that neuronal signals from intra-abdominal fat tissue are involved in food-intake regulation. In contrast, in nerve-dissected mice, blood glucose (Figure 3F) as well as serum insulin (Figure 3G) and leptin (Figure 3H) levels were significantly suppressed in a fashion similar to in sham-operated mice. Thus, improved insulin resistance is largely independent of this neuronal pathway.

To confirm that afferent-nerve signals are involved in UCP1-expression-mediated suppression of food intake, we next examined the effects of functional deafferentation by administering capsaicin (Fu et al., 2003), a selective neurotoxin for unmyelinated C fibers. In LacZ mice, food intake was not altered by capsaicin treatment 10 days prior to adenoviral administration. In contrast, capsaicin pretreatment significantly reversed the food-intake suppression induced by UCP1 expression in Epi (Figure 3I). The inhibitory effect of capsaicin pretreatment was very similar to that of local-nerve dissection (Figure 3E). Taken together, these observations suggest that afferent-nerve signals from Epi are involved in food-intake regulation. To elucidate the molecular mechanism whereby UCP1 expression in Epi modulates neuronal activity, we searched for genes upregulated by adipose UCP1 expression. Using the DNA microarray technique, gene expressions were examined in LacZ- and UCP1-adenovirus-treated Epi (Table S1) and in 3T3-L1 adipocytes (Table S2). With the exception of UCP1, however, there was no overlap in genes showing significantly increased expression. Although further expression profiling including proteomic approaches might elucidate the underlying mechanisms, the apparent lack of genes showing increased expression raises the possibility that the activation of afferent nerves does not involve gene-expression alterations. For instance, UCP1 generates heat, and a capsaicin receptor, TRPV1, is activated by a slightly above normal body temperature (Caterina et al., 1997). Capsaicin treatment affected UCP1-induced food-intake suppression (Figure 3I), raising the possibility that UCP1 expression activates capsaicin-sensitive nerves via TRPV1 activation. Another possibility is involvement of reactive oxygen species, which are affected by mitochondrial uncoupling (Bernal-Mizrachi et al., 2005; Jezek et al., 2004) and reportedly regulate capsaicin-sensitive afferent fibers (Ruan et al., 2005). Further studies are required to examine these hypotheses.

In this study, very limited UCP1 expression in Epi markedly improved insulin and leptin resistance, thereby improving glucose tolerance and decreasing food intake. UCP1 mice were more insulin sensitive than pair-fed LacZ mice. In addition, in db/db mice, despite no food-intake suppression, blood glucose

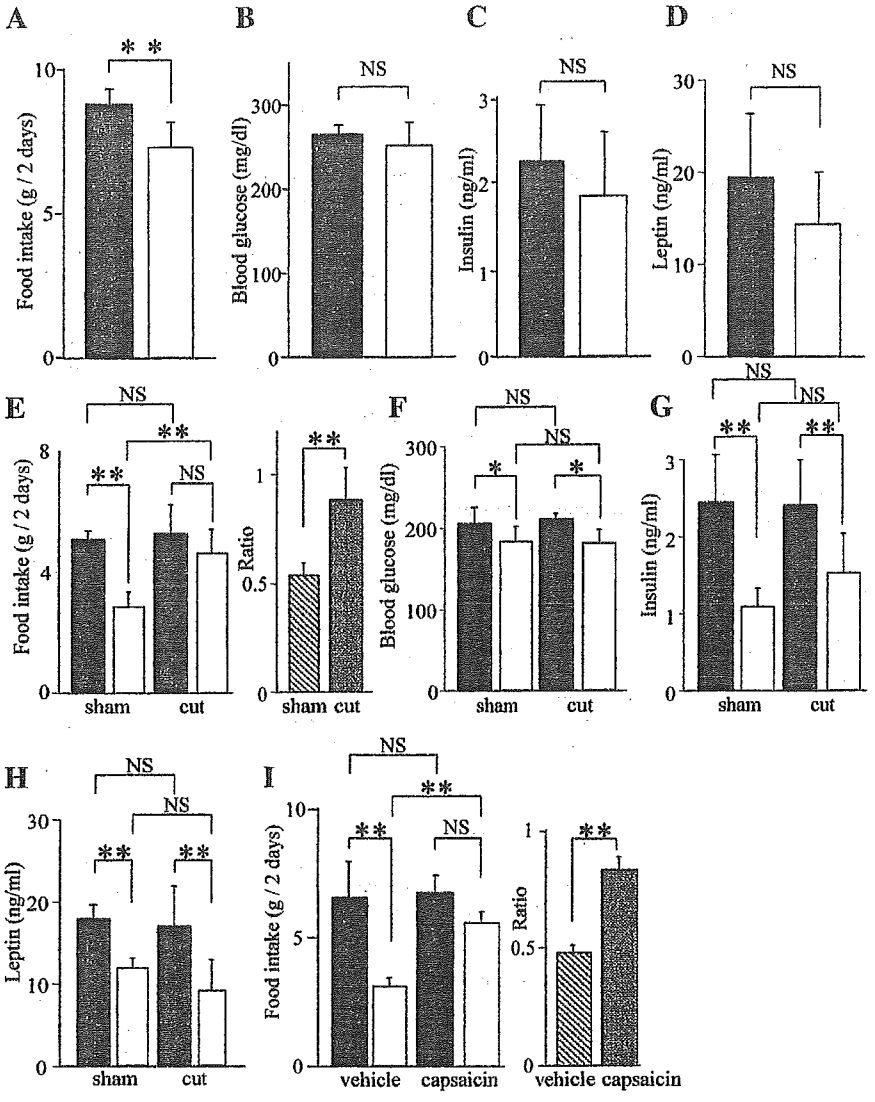

Figure 3. Neuronal signals are likely to be involved in food-intake regulation

A–D) LacZ (black bars) or UCP1 (white bars) adenovirus was injected into subcutaneous fat, and metabolic markers were measured. Total food intakes on days 2 and 3 after adenoviral administration are presented. Blood glucose **(B)**, insulin **(C)**, and leptin **(D)** levels were determined after a 10 hr fast on day 3 after adenoviral administration. $^{**}p < 0.01$ by unpaired t test.

E–H) Mice were subjected to local-nerve dissection 10 days prior to adenoviral injection into Epi. Total food intakes of sham-operated (sham) and nerve-dissected (cut) mice **(E)** on days 2 and 3 are presented graphically. Blood glucose **(F)**, serum insulin **(G)**, and leptin **(H)** levels were determined on day 3.

I) Mice were treated with capsaicin or vehicle 10 days prior to adenoviral injection into Epi. Total food intakes on days 2 and 3 after administration of LacZ (black bars) or UCP1 (white bars) adenovirus are presented. In **(E)** and **(I)**, the food intakes of UCP1 mice are expressed in the right graph as ratios to those of LacZ mice. $^{**}p < 0.01$ assessed by one-factor ANOVA. Data are presented as means ± SD.

and insulin levels were modestly but significantly decreased by UCP1 expression in Epi. Thus, the mechanism underlying improved insulin sensitivity with UCP1 expression in Epi is, in part, independent of leptin signaling and food-intake suppression (Figure 4). Dissection of the nerve bundle from Epi did not alter the decreases in blood glucose and insulin levels. Taken together with the findings that UCP1 expression in subcutaneous fat did not significantly decrease blood glucose or insulin levels, our observations indicate that nonneuronal signals including humoral factors from intra-abdominal adipose tissue possibly participate in systemic improvement of insulin resistance. Since UCP1 expression was observed in a very limited population of adipocytes in Epi, suppression of insulin-resistant adipocytokine secretion is unlikely to explain the beneficial effects. Serum adiponectin levels were not altered, suggesting involvement of other unknown insulin-sensitizing factor (or factors).

On the other hand, decreased food intake is likely to be, at least partially, mediated by afferent-nerve signals from Epi (Figure 4). Afferent-nerve signals from Epi to the central nervous system reportedly result in a reflex from epididymal fat to white adipose tissues via efferent sympathetic-nerve activation (Niijima, 1998; Tanida et al., 2000). In addition, vagal afferent

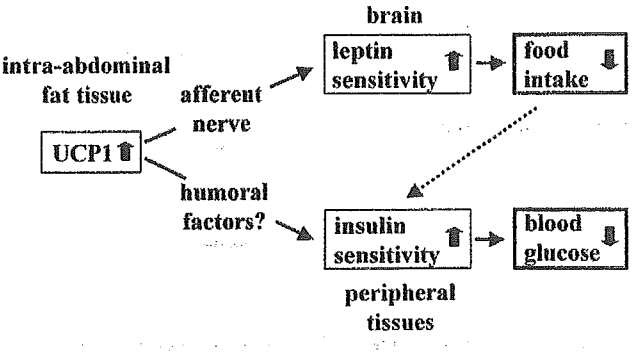

Figure 4. The proposed mechanism whereby UCP1 expression in Epi decreases food intake and improves glucose tolerance

neuronal signals from intra-abdominal tissues, including the gut (Fu et al., 2003; Smith et al., 1981) and the liver (Friedman, 1998; Scharrer, 1999), are known to play a part in regulating food intake. We also reported that UCP1 gene administration into the liver modulates food intake (Ishigaki et al., 2005). Herein we report that intra-abdominal fat tissue is likely to convey metabolic signals to the brain via a neuronal pathway, in addition to via the circulation, resulting in modulation of food intake. Although the precise molecular mechanism remains to be elucidated, this neuronal pathway might play a role in development of the metabolic syndrome, making it a potentially novel therapeutic target.

Experimental procedures

Preparation of recombinant adenovirus

Recombinant adenovirus containing murine UCP1 cDNA (Ishigaki et al., 2005) was constructed as described previously (Katagiri et al., 1996). Recombinant adenoviruses bearing the bacterial β-galactosidase gene (*Adex1CAlacZ*) and green fluorescent protein (AdCMV-GFP) were used as controls.

Animals and in vivo adenovirus injection into fat pad

Animal studies were conducted in accordance with the institutional guidelines for animal experiments at Tohoku University. Male C57BL/6N and AKR/N mice were housed individually, and high-fat-chow feeding (32% safflower oil, 33.1% casein, 17.6% sucrose, and 5.6% cellulose) (Ishigaki et al., 2005) was initiated at 5 weeks of age. After 4 weeks of high-fat-chow loading, body-weight-matched mice were anesthetized prior to dissection of the skin and body wall. The adenoviral preparation (1×10^8 plaque-forming units in a volume of 20 μl) was injected at two points each on each side of the epididymal fat pad or subcutaneous fat tissues in the flank, i.e., a total of four points. KK mice and KK-Ay mice maintained on a standard diet (65% carbohydrate, 4% fat, 24% protein) were similarly administered adenoviruses at 9 weeks and 5 weeks of age, respectively.

Immunoblotting

Tissue protein extracts (250 μg total protein) were boiled in Laemmli buffer containing 10 mM dithiothreitol, subjected to SDS-polyacrylamide gel electrophoresis, and transferred onto nitrocellulose filters. The filters were incubated with anti-UCP1 antibody (Santa Cruz Biotechnology, Santa Cruz, California) and then with anti-goat immunoglobulin G coupled to horseradish peroxidase. The immunoblots were visualized with an enhanced chemiluminescence detection kit (Amersham, Buckinghamshire, UK). The intensities of bands were quantified with the NIH Image 1.62 program.

Histological analysis

Mouse epididymal fat and BAT were immunostained as previously reported (Ishigaki et al., 2005). Mature white adipocytes were identified by their characteristic unilocular appearance. Diameters of 100 or more white adipocytes per mouse in each group were traced manually and analyzed.

Oxygen consumption

Oxygen consumption was measured as previously reported (Ishigaki et al., 2005).

Pair-feeding experiments

Pair-feeding experiments were performed as previously described (Ishigaki et al., 2005).

Blood analysis

Blood glucose and serum insulin, leptin, adiponectin, TNFα, total cholesterol, triglyceride, and free-fatty-acid levels were determined as previously described (Ishigaki et al., 2005).

Measurement of quantitative RT-PCR-based gene expression

The skull was reflected from the brain and the hypothalamus was isolated by snap freezing in liquid nitrogen as previously reported (Bjorbaek et al., 1998). Total RNA was isolated from mouse hypothalamus, fat tissues, or 3T3-L1 adipocytes with ISOGEN (Wako Pure Chemical Co., Osaka, Japan), and cDNA synthesized from total RNA was evaluated with a real-time PCR quantitative system (Light Cycler Quick System 350S; Roche Diagnostics GmbH, Mannheim, Germany).The relative amount of mRNA was calculated with β-actin mRNA as the invariant control. The primers used are shown in Table S3.

Glucose-, insulin-, and leptin-tolerance tests

Glucose-tolerance tests were performed on fasted (10 hr, daytime) mice. Mice were given glucose (2 g/kg of body weight) intraperitoneally, followed by measurement of blood glucose levels. Insulin-tolerance tests were performed on ad libitum-fed mice. Mice were intraperitoneally injected with human regular insulin (0.75 U/kg of body weight; Eli Lilly Co., Kobe, Japan).

Leptin-tolerance tests were carried out as described in a previous report (Igel et al., 1997), with slight modification. Fasted (12 hr) mice were injected with mouse leptin (7.2 mg/kg of body weight; R&D Systems, Inc.) intraperitoneally, and food intakes were monitored for 12 hr after the injection. To examine effects on body-weight change, these two groups of mice were given leptin daily starting on the day of adenoviral administration. Each mouse was then weighed.

Capsaicin treatments

Capsaicin treatment was performed as described in a previous report (Fu et al., 2003), with minor modification. Mice were anesthetized prior to subcutaneous injection of capsaicin solution (50 mg/kg, 12.5 mg/ml dissolved in vehicle). The control group received vehicle treatment (10% Tween 80, 10% ethanol, and 80% saline) under identical administration conditions. Adenoviral administration into Epi was carried out 10 days later.

Local-nerve dissection

The small nerve bundle which runs along side blood vessels supplying Epi was dissected as previously reported (Niijima, 1998). Ten days after bilateral dissection of this nerve bundle, adenoviruses were injected into epididymal fat pad.

Measurement of ATP

Fully differentiated 3T3-L1 adipocytes were infected with recombinant adenoviruses as previously described (Katagiri et al., 1996). Intracellular ATP levels were measured using an ATP determination kit (TOYO B-Net, Tokyo, Japan).

Microarray experiments

Total RNA from epididymal fat or 3T3-L1 adipocytes was used to synthesize cRNA, which was then hybridized to an HG-U133A oligonucleotide array (Affymetrix, Santa Clara, California) according to standard protocols, as described previously (Hippo et al., 2002).

Statistical analysis

All data were expressed as means ± SD. The statistical significance of differences was assessed by the unpaired t test and one-factor ANOVA.

Supplemental data

Supplemental Data include four figures and three tables and can be found with this article online at http://www.cellmetabolism.org/cgi/content/full/3/3/223/DC1/.

Acknowledgments

We appreciate Drs. L.P. Kozak (Pennington Biomedical Research Center) and H. Mizuguchi (National Institute of Biomedical Innovation) for the generous gifts of UCP1 cDNA and GFP-adenovirus, respectively. We thank Ms. H. Meguro (Tokyo University) for technical support. This work was supported by a Grant-in-Aid for Scientific Research (B2, 15390282) and a Grant-in-Aid for Exploratory Research (15659214) to H.K. from the Ministry of Education, Science, Sports and Culture of Japan and a Grant-in-Aid for Scientific Research (H16-genome-003) to Y.O. from the Ministry of Health, Labor and Welfare of Japan. This work was also supported by the 21st Century COE Programs "CRESCENDO" (H.K.) and "the Center for Innovative Therapeutic Development for Common Diseases" (Y.O.) of the Ministry of Education, Science, Sports and Culture.

Received: June 22, 2005
Revised: October 12, 2005
Accepted: February 1, 2006
Published: March 7, 2006

References

Bernal-Mizrachi, C., Gates, A.C., Weng, S., Imamura, T., Knutsen, R.H., DeSantis, P., Coleman, T., Townsend, R.R., Muglia, L.J., and Semenkovich, C.F. (2005). Vascular respiratory uncoupling increases blood pressure and atherosclerosis. Nature *435*, 502–506.

Bjorbaek, C., Elmquist, J.K., Frantz, J.D., Shoelson, S.E., and Flier, J.S. (1998). Identification of SOCS-3 as a potential mediator of central leptin resistance. Mol. Cell *1*, 619–625.

Bjorntorp, P. (1992). Abdominal fat distribution and disease: an overview of epidemiological data. Ann. Med. *24*, 15–18.

Caterina, M.J., Schumacher, M.A., Tominaga, M., Rosen, T.A., Levine, J.D., and Julius, D. (1997). The capsaicin receptor: a heat-activated ion channel in the pain pathway. Nature *389*, 816–824.

Cederberg, A., Gronning, L.M., Ahren, B., Tasken, K., Carlsson, P., and Enerback, S. (2001). FOXC2 is a winged helix gene that counteracts obesity, hypertriglyceridemia, and diet-induced insulin resistance. Cell *106*, 563–573.

Considine, R.V., Sinha, M.K., Heiman, M.L., Kriauciunas, A., Stephens, T.W., Nyce, M.R., Ohannesian, J.P., Marco, C.C., McKee, L.J., Bauer, T.L., et al. (1996). Serum immunoreactive-leptin concentrations in normal-weight and obese humans. N. Engl. J. Med. *334*, 292–295.

Flier, J.S. (2004). Obesity wars: molecular progress confronts an expanding epidemic. Cell *116*, 337–350.

Friedman, J.M. (2003). A war on obesity, not the obese. Science *299*, 856–858.

Friedman, J.M., and Halaas, J.L. (1998). Leptin and the regulation of body weight in mammals. Nature *395*, 763–770.

Friedman, M.I. (1998). Fuel partitioning and food intake. Am. J. Clin. Nutr. *67*, 513S–518S.

Fu, J., Gaetani, S., Oveisi, F., Lo Verme, J., Serrano, A., Rodriguez De Fonseca, F., Rosengarth, A., Luecke, H., Di Giacomo, B., Tarzia, G., and Piomelli, D. (2003). Oleylethanolamide regulates feeding and body weight through activation of the nuclear receptor PPAR-alpha. Nature *425*, 90–93.

Heymsfield, S.B., Greenberg, A.S., Fujioka, K., Dixon, R.M., Kushner, R., Hunt, T., Lubina, J.A., Patane, J., Self, B., Hunt, P., and McCamish, M. (1999). Recombinant leptin for weight loss in obese and lean adults: a randomized, controlled, dose-escalation trial. JAMA *282*, 1568–1575.

Hippo, Y., Taniguchi, H., Tsutsumi, S., Machida, N., Chong, J.M., Fukayama, M., Kodama, T., and Aburatani, H. (2002). Global gene expression analysis of gastric cancer by oligonucleotide microarrays. Cancer Res. *62*, 233–240.

Igel, M., Becker, W., Herberg, L., and Joost, H.G. (1997). Hyperleptinemia, leptin resistance, and polymorphic leptin receptor in the New Zealand obese mouse. Endocrinology *138*, 4234–4239.

Ishigaki, Y., Katagiri, H., Yamada, T., Ogihara, T., Imai, J., Uno, K., Hasegawa, Y., Gao, J., Ishihara, H., Shimosegawa, T., et al. (2005). Dissipating excess energy stored in the liver is a potential treatment strategy for diabetes associated with obesity. Diabetes *54*, 322–332.

Jezek, P., Zackova, M., Ruzicka, M., Skobisova, E., and Jaburek, M. (2004). Mitochondrial uncoupling proteins—facts and fantasies. Physiol. Res. *53* Suppl. 1, S199–S211.

Katagiri, H., Asano, T., Ishihara, H., Inukai, K., Shibasaki, Y., Kikuchi, M., Yazaki, Y., and Oka, Y. (1996). Overexpression of catalytic subunit p110alpha of phosphatidylinositol 3-kinase increases glucose transport activity with translocation of glucose transporters in 3T3-L1 adipocytes. J. Biol. Chem. *271*, 16987–16990.

Klingenberg, M., and Huang, S.G. (1999). Structure and function of the uncoupling protein from brown adipose tissue. Biochim. Biophys. Acta *1415*, 271–296.

Kopecky, J., Clarke, G., Enerback, S., Spiegelman, B., and Kozak, L.P. (1995). Expression of the mitochondrial uncoupling protein gene from the aP2 gene promoter prevents genetic obesity. J. Clin. Invest. *96*, 2914–2923.

Leonardsson, G., Steel, J.H., Christian, M., Pocock, V., Milligan, S., Bell, J., So, P.W., Medina-Gomez, G., Vidal-Puig, A., White, R., and Parker, M.G. (2004). Nuclear receptor corepressor RIP140 regulates fat accumulation. Proc. Natl. Acad. Sci. USA *101*, 8437–8442.

Matsuzawa, Y., Shimomura, I., Nakamura, T., Keno, Y., and Tokunaga, K. (1995). Pathophysiology and pathogenesis of visceral fat obesity. Ann. N Y Acad. Sci. *748*, 399–406.

Niijima, A. (1998). Afferent signals from leptin sensors in the white adipose tissue of the epididymis, and their reflex effect in the rat. J. Auton. Nerv. Syst. *73*, 19–25.

Ruan, T., Lin, Y.S., Lin, K.S., and Kou, Y.R. (2005). Sensory transduction of pulmonary reactive oxygen species by capsaicin-sensitive vagal lung afferent fibres in rats. J. Physiol. *565*, 563–578.

Scharrer, E. (1999). Control of food intake by fatty acid oxidation and ketogenesis. Nutrition *15*, 704–714.

Smith, G.P., Jerome, C., Cushin, B.J., Eterno, R., and Simansky, K.J. (1981). Abdominal vagotomy blocks the satiety effect of cholecystokinin in the rat. Science *213*, 1036–1037.

Tanida, M., Iwashita, S., Ootsuka, Y., Terui, N., and Suzuki, M. (2000). Leptin injection into white adipose tissue elevates renal sympathetic nerve activity dose-dependently through the afferent nerves pathway in rats. Neurosci. Lett. *293*, 107–110.

Tsukiyama-Kohara, K., Poulin, F., Kohara, M., DeMaria, C.T., Cheng, A., Wu, Z., Gingras, A.C., Katsume, A., Elchebly, M., Spiegelman, B.M., et al. (2001). Adipose tissue reduction in mice lacking the translational inhibitor 4E-BP1. Nat. Med. *7*, 1128–1132.

Um, S.H., Frigerio, F., Watanabe, M., Picard, F., Joaquin, M., Sticker, M., Fumagalli, S., Allegrini, P.R., Kozma, S.C., Auwerx, J., and Thomas, G. (2004). Absence of S6K1 protects against age- and diet-induced obesity while enhancing insulin sensitivity. Nature *431*, 200–205.

Journal of Infection (2005) 50, 394-396

ELSEVIER

BRITISH INFECTION SOCIETY

www.elsevierhealth.com/journals/jinf

Cerebroventricular infusion of pentosan polysulphate in human variant Creutzfeldt-Jakob disease

N.V. Todd[a], J. Morrow[b], K. Doh-ura[c], S. Dealler[d], S. O'Hare[e], P. Farling[f], M. Duddy[b], N.G. Rainov[g,*]

[a]*Regional Neurosciences Centre, Newcastle General Hospital NHS Trust, Newcastle, UK*
[b]*Department of Neurology, Royal Victoria Hospital, Belfast, UK*
[c]*Department of Prion Research, Tohoku University Graduate School of Medicine, Japan*
[d]*Department of Microbiology, Lancaster General Infirmary; Lancaster, UK*
[e]*Department of Pharmacy, Royal Victoria Hospital, Belfast, UK*
[f]*Department of Anesthetics, Royal Victoria Hospital, Belfast, UK*
[g]*Department of Neurological Science, The University of Liverpool, and The Walton Centre for Neurology and Neurosurgery NHS Trust, Lower Lane, Liverpool L9 7LJ, UK*

Accepted 24 July 2004
Available online 22 September 2004

KEYWORDS
Brain;
Intraventricular;
New variant CJD;
Pentosan polysulphate

Abstract Variant Creutzfeldt-Jakob disease (CJD) is a transmissible spongiform encephalopathy believed to be caused by the bovine spongiform encephalopathy agent, an abnormal isoform of the prion protein (PrP^{sc}). At present there is no specific or effective treatment available for any form of CJD. Pentosan polysulphate (PPS), a large polyglycoside molecule with weak heparin-like activity, has been shown to prolong the incubation period of the intracerebral infection when administered to the cerebral ventricles in a rodent scrapie model. PPS also prevents the production of further PrP^{sc} in cell culture models.

These properties of PPS prompted its cerebroventricular administration in a young man with vCJD. Long-term continuous infusion of PPS at a dose of 11 μg/kg/day for 18 months did not cause drug-related side effects. Follow-up CT scans demonstrated progressive brain atrophy during PPS administration. Further basic and clinical research is needed in order to address the issue of efficacy of PPS in vCJD and in other prion diseases.

Introduction

Variant Creutzfeldt-Jakob disease (vCJD) is a form of CJD believed to be caused by the bovine spongiform encephalopathy agent.[1-3] Unlike the

* Corresponding author. Tel.: +44-151-529-5323; fax: +44-151-529-5465.
E-mail address: rainov@liv.ac.uk (N.G. Rainov).

0163-4453/$30.00
doi:10.1016/j.jinf.2004.07.015

sporadic form, vCJD mostly becomes symptomatic in young adults and adolescents.[1] Pentosan polysulphate (PPS) is a large polyglycoside molecule with weak heparin-like activity. It has been shown to prevent the propagation of the abnormal isoform of the prion protein (PrP^{sc}) in cell culture models,[4] and to prolong the incubation period of intracerebral infection in rodent scrapie models when administered either systemically[5] or directly into the cerebral ventricles.[6] These properties of PPS prompted our use of cerebroventricular PPS in escalating doses in one patient with vCJD to assess the safety and tolerability of the drug when administered by this route.

Case report and discussion

The patient is a 20-year-old man who presented initially at the age of 16 years and 11 months with subjective signs of behavioural disturbance. A few months later this was followed by progressive ataxia, pyramidal signs and myoclonus, which led to the clinical diagnosis of possible vCJD. The clinical picture combined with abnormal MR findings in the FLAIR sequence (pulvinar sign) and positive tonsil biopsy allowed the diagnosis of probable vCJD 8 months after the initial clinical symptoms (Fig. 1). At the time of initial administration of PPS (Pentosan polysulphate SP54, Bene Arzneimittel GmbH, Munich, Germany) into the cerebral ventricular system, the patient had symptoms of advanced vCJD,[7] such as ataxia, dementia, dysphagia, dysphasia, myoclonus, and was confined to bed and unable to care for himself. He was fed via percutaneous gastrostomy.

A permanently implanted right frontal intraventricular catheter was connected to a subcutaneous programmable pump (Synchromed EL, Medtronic Inc.). The initial PPS dose of 1 μg/kg/d was escalated without significant problem to the target dose, extrapolated from animal studies, of 11 μg/kg/d. A possible therapeutic dose-effect relationship for intracerebroventricular PPS in humans with prion disease remains unknown, and therefore further dose escalation would only be limited by side effects. In mice, dose-response studies with PPS have shown that the most effective dose is 230 μg/kg/d.[6] In our current human dosing this would translate to 23 μg/kg/d, which is a little more than twice the current daily dose of PPS.

Continuous infusion of PPS for 18 months did not cause any drug-related side effects. Cerebroventricular PPS at the above dose did not have any measurable systemic anticoagulant activity in serum, as confirmed by unchanged INR (international normalised ratio) before and during PPS infusion.

Follow-up CT scans demonstrated no intracerebral haemorrhage (Fig. 2), and there were no seizures. A right parietal subdural fluid collection of increasing size was noted on CT scans 8 months after start of PPS infusion and necessitated surgical (burr hole) evacuation of fluid. PPS infusion was halted temporarily and restarted one week after the surgery. Due to recurrent subdural fluid collections, two further surgical revisions were necessary.

Clearly comments on efficacy are difficult in the setting of a single case, but after 18 months of continuous cerebroventricular PPS administration, the patient is still alive and there is some evidence of a change in the neurological condition. He is now able to fix his eyes on persons, to obey simple one stage commands, and to make verbalization attempts in response to stimuli. The sleep/wake cycle and the reflex swallow are restored and the

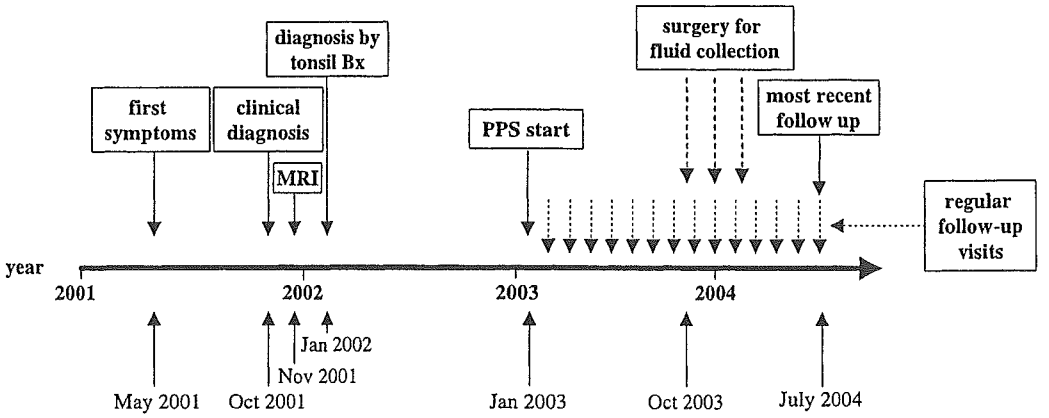

Figure 1 Schematic representation of the time course of disease presentation, diagnosis and management. Bx = biopsy.

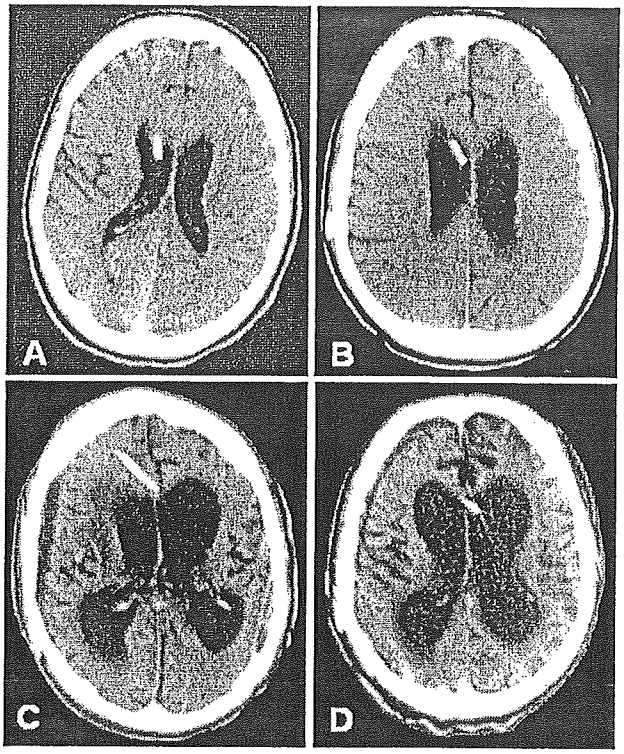

Figure 2 (A) Non-enhanced CT scan on day 6 after start of cerebroventricular PPS infusion. (B) Non-enhanced CT scan 3 months after start of PPS infusion. Note the slightly enlarged lateral ventricles compared to baseline (A). (C) Non-enhanced CT scan 1-year after start of PPS infusion. (D) Non-enhanced CT scan 15 months after start of PPS infusion. Note progressing cortical and subcortical atrophy with enlargement of the ventricular system on scans C and D.

myoclonus is reduced. The patient has gained 5 kg of weight compared to pre-PPS baseline, while on the same nutritional regime. Regular follow-up observations and pump refills (every 6 weeks) were carried out by the same medical and nursing staff and physiotherapists involved with the patient's care from the early stages of his disease. Despite the apparent trend towards clinical improvement, brain atrophy, as seen on regular follow-up CT scans, continued to progress during the period of PPS administration and resulted in ventriculomegaly and grossly enlarged extracerebral CSF spaces (Fig. 2).

In conclusion, cerebroventricular infusion of PPS at 11 μg/kg/d appears safe and well tolerated for continuous long-term application. Our patient has survived for 37 months after initial symptoms and 30 months after diagnosis of probable vCJD, while the median duration of illness with vCJD is 13 months (range 6-39)[7].

Further lessons have also been learned from this first case. Firstly, surgery in a brain affected by vCJD may result in a higher rate of surgical complications than might be expected in a normal patient. We suggest that in order to allow the catheter track to organise, drug infusion should be delayed for at least 7-10 days after implantation of the pump system. Regular neuroradiological follow-up throughout the treatment period is strongly recommended. Secondly, if clinically significant benefits are to be expected, PPS administration should start as early as possible in the course of the disease and before irreversible loss of neurological function has occurred.

Further clinical, neuroradiological and laboratory investigations in the setting of a prospective clinical study with standardised follow-up protocol and data collection are essential in order to assess the efficacy of PPS administration in vCJD and in other prion diseases.

Acknowledgements

The authors would like to thank Dr R. Knight (Edinburgh) and Dr C. Pomfrett (Manchester) for useful comments and suggestions regarding the manuscript. Dr M. McClean (Belfast) is gratefully acknowledged for his general medical input and practical support.

References

1. Will RG, Ironside JW, Zeidler M, Cousens SN, Estibeiro K, Alperovitch A, Poser S, Pocchiari M, Hofman A, Smith PG. A new variant of Creutzfeldt-Jakob disease in the UK. *Lancet* 1996;**347**:921-5.
2. Bruce ME, Will RG, Ironside JW, McConnell I, Drummond D, Suttie A, McCardle L, Chree A, Hope J, Birkett C, Cousens S, Fraser H, Bostock CJ. Transmissions to mice indicate that 'new variant' CJD is caused by the BSE agent. *Nature* 1997; **389**:498-501.
3. Hill AF, Desbruslais M, Joiner S, Sidle KC, Gowland I, Collinge J, Doey LJ, Lantos P. The same prion strain causes vCJD and BSE. *Nature* 1997;**389**:448-50.
4. Caughey B, Raymond GJ. Sulfated polyanion inhibition of scrapie-associated PrP accumulation in cultured cells. *J Virol* 1993;67:643-50.
5. Ladogana A, Casaccia P, Ingrosso L, Cibati M, Salvatore M, Xi YG, Masullo C, Pocchiari M. Sulphate polyanions prolong the incubation period of scrapie infected hamsters. *J Gen Virol* 1992;**73**:661-5.
6. Doh-ura K, Ishikawa K, Murakami-Kubo I, Sasaki K, Mohri S, Race R, Iwaki T. Treatment of transmissible spongiform encephalopathy by intraventricular drug infusion in animal models. *J Virol* 2004;**78**:4999-5006.
7. Henry C, Knight R. Clinical features of variant Creutzfeldt-Jakob disease. *Rev Med Virol* 2002;**12**:143-50.

ELSEVIER

Journal of the Neurological Sciences 232 (2005) 45–49

Journal of the Neurological Sciences

www.elsevier.com/locate/jns

Diffusion-weighted MRI in familial Creutzfeldt–Jakob disease with the codon 200 mutation in the prion protein gene

Yoshio Tsuboi[a,*], Yasuhiko Baba[b], Katsumi Doh-ura[c], Akiko Imamura[a], Shinsuke Fujioka[a], Tatsuo Yamada[a]

[a]*Fifth Department of Internal Medicine, Fukuoka University School of Medicine, 7-45-1 Nanakuma, Johnan-ku, Fukuoka 814-0180, Japan*
[b]*Department of Neurology, Mayo Clinic Jacksonville, Florida, USA*
[c]*Department of Prion Research, Tohoku University, Sendai, Japan*

Received 28 July 2004; received in revised form 11 January 2005; accepted 12 January 2005
Available online 25 February 2005

Abstract

Magnetic resonance imaging (MRI) with diffusion-weighted imaging (DWI) has been reported to be a useful tool for early diagnosis of sporadic Creutzfeldt–Jakob disease (CJD). We report MRI findings with DWI, as well as with fluid-attenuated inversion recovery (FLAIR) and T1-weighted imaging (T1WI), in a case of familial CJD with a mutation at codon 200 of the prion protein gene. DWI in this patient showed high signal intensity in the basal ganglia and the cerebral cortex, similar to findings in sporadic CJD. In addition, T1WI showed areas of high signal intensity bilaterally in the globus pallidus. Despite the clinical diversity and atypical laboratory findings seen in familial CJD with the codon 200 mutation, these neuroimaging studies suggest that common regional distributions and a common pathogenesis might underlie the clinical progression both in sporadic CJD and in familial CJD with the codon 200 mutation in the prion protein gene. DWI abnormalities may be characteristic features that should be considered in the diagnosis of familial as well as of sporadic CJD.

Keywords: Creutzfeldt–Jakob disease; Diagnostic methods; Diffusion-weighted imaging; Familial; Magnetic resonance imaging; Prion disease; Prion gene mutation

1. Introduction

Creutzfeldt–Jakob disease (CJD) is a rare and fatal neurodegenerative disorder caused by abnormal prion protein accumulation in the brain [1–3]. CJD may occur in sporadic, infectious, or familial forms. The familial form is found in 10% to 15% of all cases of CJD [4]. The diagnosis of CJD is usually based on clinical features, characteristic electroencephalographic (EEG) activity, and laboratory values. The clinical features consist of rapidly progressive dementia, myoclonus, and ataxia and are typically fatal within 1 year from the onset of symptoms [1–3]. EEG activity in CJD is characterized by periodic sharp and slow wave complexes [5]. Laboratory criteria include an elevated concentration of neuron-specific enolase (NSE) and the presence of 14–3–3 protein in the cerebrospinal fluid (CSF) [5–8].

Diagnosis of familial CJD is often difficult because clinical presentation varies widely, and characteristic features are not always present [6,9]. Familial CJD can be caused by several different mutations in the prion protein gene [4]. Atypical clinical features may be related to different genotypes at codon 129 or 219 [10,11]. One mutation at codon 200 in the prion protein gene is known to present with diverse clinical characteristics ranging from features similar to those of sporadic CJD [12–15] to atypical features such as slow progression of symptoms, fatal insomnia, polyneuropathy, lack of characteristic EEG

* Corresponding author. Tel.: +81 92 801 1011; fax: +81 92 865 7900.
E-mail address: tsuboi@cis.fukuoka-u.ac.jp (Y. Tsuboi).

0022-510X/$ - see front matter © 2005 Elsevier B.V. All rights reserved.
doi:10.1016/j.jns.2005.01.006

abnormalities, and absence of 14–3–3 protein in the CSF [10,16,17].

Thus, a useful diagnostic tool is needed, particularly for patients without a known family history of CJD. The presence of 14–3–3 protein in the CSF has been recognized to have good sensitivity and specificity as an indicator of sporadic CJD [5–7,18]. However, no studies have been published on the sensitivity and specificity of CSF abnormalities in familial CJD, and as many as 25% of patients with familial CJD may have normal 14–3–3 protein and NSE concentrations in the CSF [5,6].

Magnetic resonance imaging (MRI) has been reported to be a useful tool for early diagnosis of sporadic CJD. For example, MRI with diffusion-weighted images (DWI) shows increased signals in the basal ganglia and cerebral cortex of patients with sporadic CJD [19–28]. Whether MRI is equally useful in the diagnosis of familial CJD remains unclear, although several MRI studies have been reported in familial CJD with various mutations in the prion protein gene [29–32].

To further investigate whether MRI might be useful in the diagnosis of familial CJD, we examined the brain of a patient with familial CJD in whom the codon 200 mutation was confirmed by molecular genetic analysis. DWI, fluid-attenuated inversion recovery (FLAIR) imaging, and T1-weighted imaging (T1WI) were performed, and the results were compared with findings in the literature on patients with sporadic CJD.

2. Case report

2.1. Clinical description

A 64-year-old right-handed woman born in southern Japan was admitted to our hospital because of forgetfulness, dysarthria, and impaired balance. She had noticed the forgetfulness and insomnia 3 months before admission. Fatigue, motor slowness, and dysarthria had developed 2 months before admission. The frequency of spontaneous speech had gradually decreased, and she had increasingly experienced loss of balance, leading to falls. The patient's mother died at age 55 of a progressive dementing disorder, and her younger sister had received a diagnosis of familial CJD at another hospital.

At admission to our hospital, the patient was alert and cooperative, but inattentive. She was able to follow simple commands, and her Mini-Mental State Examination (MMSE) score at that time was 23 of 30 possible points. Her speech was slurred, and scanning speech was occasionally evident. Her pupils were normal in size and reacted to light stimulation. Extraocular movement was normal. Cerebellar ataxia was detected, including dysmetria and decomposition in all extremities. Her gait was also ataxic and wide based. No involuntary movements were observed. She did not smoke or consume alcohol and had no history of toxic exposure. Results of extensive laboratory evaluations of serum, urine, and CSF were normal, except for positive

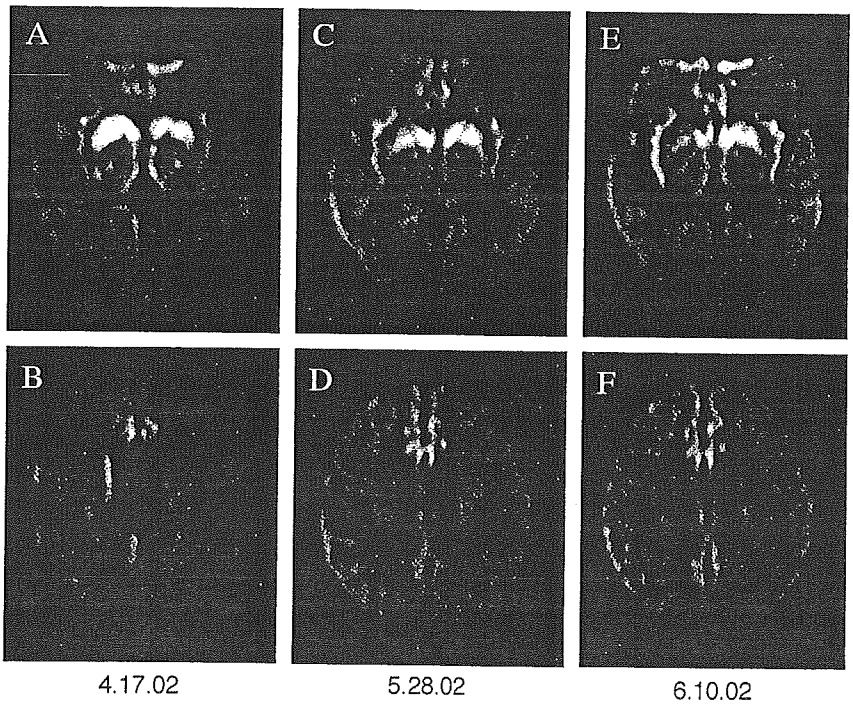

Fig. 1. Magnetic resonance imaging of the brain of a patient with familial Creutzfeldt–Jakob disease, performed with serial diffusion-weighted images (DWI). (A) and (B) were performed at admission to hospital, (C) and (D) at approximately 1 month, and (E) and (F) at 2 months after admission. (A) and (B) High signal intensity bilaterally in the basal ganglia, insula, and cingulate gyrus. (C) and (D) Slightly decreased hyperintense bilateral signals in the basal ganglia; extension of signals in the cortex into left temporoparietal cortex and cingulate gyrus. (C) Increased signal intensity in areas of hyperintensity in insular cortex. (E) and (F) Slight decrease in hyperintense signals in cingulate gyrus, insular cortex, left temporoparietal cortex, and basal ganglia.

14–3–3 protein (+; normal, negative) and elevated NSE (77 ng/mL; normal, <35 ng/mL) in the CSF. At that time, EEG showed diffuse slow waves without periodic sharp waves.

A diagnosis of familial CJD was made, and treatment with quinacrine was started at 300 mg/day. Despite treatment, the patient's speech and gait deteriorated rapidly. Her cognitive decline also progressed rapidly in association with myoclonic jerks in the upper extremities. Subsequently, both spontaneous and stimulus-induced episodes of myoclonus were seen in all extremities. Rigidity, Babinski signs, snout reflex, and bilateral grasping reflex also developed. One month after admission (4 months after the onset of symptoms), EEG showed diffuse slow and periodic sharp-wave complex discharges.

Genomic DNA was extracted from peripheral lymphocytes. The coding sequence of the prion protein gene was amplified by using polymerase chain reaction. Genetic study confirmed the point mutation at codon 200 (GAG→AAG) resulting in the substitution of lysine for glutamate.

2.2. Magnetic resonance imaging studies

MRI of the brain was performed with DWI, FLAIR imaging, and T1WI at admission, as well as approximately 1 and 2 months later.

At admission, DWI demonstrated high signal intensity bilaterally in the basal ganglia, insula, and cingulate gyrus (Fig. 1A and B). FLAIR imaging also showed high signal intensity bilaterally in the basal ganglia (Fig. 2A). Apparent diffusion coefficient (ADC) mapping of these regions revealed decreased signal intensity, indicating cytotoxic edema. T1-weighted imaging (T1WI) showed normal results (Fig. 2B).

DWI performed approximately 1 month after admission showed that the hyperintense signals in the basal ganglia had decreased slightly and those in the cortex had extended into the left temporoparietal cortex and the cingulate gyrus (Fig. 1C and D). DWI also showed that the hyperintensity in the insular cortex had increased in signal intensity (Fig. 1C). On T1WI, spotty hyperintense signals had appeared bilaterally in the globus pallidus (Fig. 2D).

On DWI performed 2 months after admission, the degree of hyperintensity in regions involving the cingulate gyrus, insular cortex, left temporoparietal cortex, and basal ganglia had decreased slightly (Fig. 1E and F). On T1WI, the increased signal intensity in the globus pallidus was more apparent than it had been 1 month after admission (Fig. 2F).

3. Discussion

The case we describe helps to clarify the role of MRI as a diagnostic tool in patients with familial CJD. Familial CJD with the codon 200 mutation was confirmed by genetic

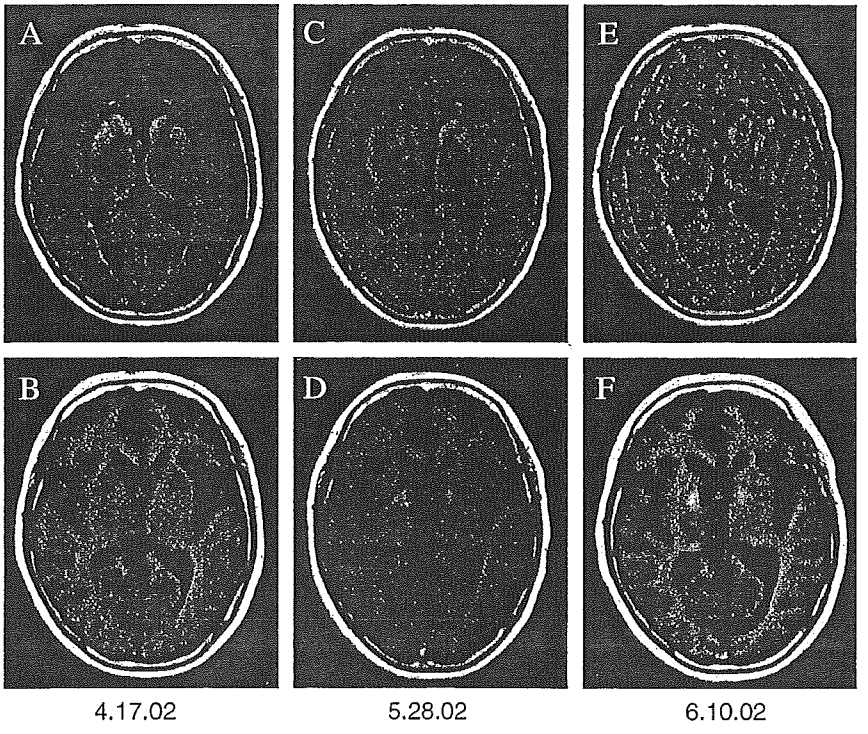

Fig. 2. Magnetic resonance imaging of the brain with serial fluid-attenuated inversion recovery (FLAIR) and T1-weighted imaging (T1WI). (A) and (B) were performed at admission, (C) and (D) at approximately 1 month, and (E) and (F) at 2 months after admission. (A) Hyperintense signals in the bilateral basal ganglia on FLAIR image. (B) Normal T1WI. (C) Slightly decreased hyperintense signals in the bilateral basal ganglia on FLAIR image. (D) Bilateral spotty hyperintense signals in the globus pallidus on T1WI. (E) No significant signal change in FLAIR (compared with FLAIR image at 1 month), but artifact prevented precise evaluation. (F) Increased signal intensity in the globus pallidus on T1WI (more apparent than at 1 month).

study in our patient. As has also been reported for other patients with this mutation [10,12–17], progression was more aggressive in our patient than in those with sporadic CJD. However, most clinical features of our case were similar to those of sporadic CJD, including rapidly progressive ataxia, severe mental deterioration, myoclonus, and typical periodic sharp-wave activity on EEG approximately 4 months after the onset of symptoms.

DWI abnormalities in our patient were observed as areas of high signal intensity in the putamen and caudate nucleus and as ribbon-like areas of hyperintensity in the cortical areas, predominantly in the insula, cingulate gyrus, and temporoparietal lobe. Although corresponding FLAIR images showed some hyperintensity in the basal ganglia, ADC mapping performed at the same time showed reduced signals in the corresponding regions, indicating that T2 shine-through contributed to the hyperintensity in the DWI only to a slight degree. The abnormalities found in our patient resemble those observed in sporadic CJD [19–28], demonstrating that similar MRI abnormalities can be found in both forms of the disease.

DWI appears to be a valuable tool that should be included in the diagnostic criteria for CJD [33]. Marked DWI changes can be observed in the early stages of symptomatic onset and are sustained over several months, although the high signal intensity seen on DWI may disappear over time in patients with advanced sporadic CJD (unpublished data). Shiga et al. [33] concluded that DWI was a more sensitive test for the early clinical diagnosis of CJD than periodic sharp wave complexes on EEG, detection of CSF 14–3–3 protein, or increase of NSE in the CSF. DWI may detect areas of increased signal intensity in the basal ganglia and cerebral cortex with greater sensitivity than that of routine MRI sequences such as T1WI, T2WI, or FLAIR images [18,34].

The pathogenesis of DWI abnormalities in the basal ganglia and cerebral cortex in CJD is not well understood. Spongiform neuronal degeneration and microglial activation might contribute to the changes demonstrated on DWI [35,36]. Cambier et al. [37] have suggested that high signal intensity on DWI may be related to periodic sharp-wave complex discharges on EEG. The EEG did not show specific changes corresponding to the DWI abnormalities in our case. Although our patient showed positive 14–3–3 protein and increased NSE in the CSF, as in sporadic CJD, it is unclear whether these findings are also related to the DWI abnormalities.

T1WI signals in the globus pallidus were initially normal in our patient and increased in intensity bilaterally during the early stages. This phenomenon might represent rapid pathologic changes in the basal ganglia during the course of the illness, corresponding to the hyperintensities shown on DWI. Such changes have previously been reported in only 1 patient with sporadic CJD, who showed typical clinical characteristics [38]. Although the high T1WI signal intensity in the globus pallidus may have been due to accumulation of prion protein in the brain [38], increased metal concentration can also cause high signal intensity on T1WI [39]. It remains doubtful whether T1WI abnormalities are pathognomonic for either sporadic or familial CJD.

To our knowledge, this is the first report to of MRI showing DWI and T1WI abnormalities in familial CJD with a point mutation at codon 200. Despite the clinical diversity and atypical laboratory findings seen in familial CJD with the codon 200 mutation, these neuroimaging studies suggest that common regional distributions and a common pathogenesis might underlie the clinical progression in both sporadic and familial CJD with the codon 200 mutation in the prion protein gene. Thus, DWI abnormalities may be characteristic features that should be considered in the diagnosis of familial as well as of sporadic CJD.

References

[1] Brown P, Cathala F, Castaigne P, Gajdusek DC. Creutzfeldt–Jakob disease: clinical analysis of a consecutive series of 230 neuropathologically verified cases. Ann Neurol 1986;20:597–602.
[2] Johnson RT, Gibbs CJ. Creutzfeldt–Jakob disease and related transmissible spongiform encephalopathies. N Engl J Med 1998;339:1994–2004.
[3] Richardson EP, Masters CL. The nosology of Creutzfeldt–Jakob disease and conditions related to the accumulation of PrP^{CJD} in the nervous system. Brain Pathol 1995;5:33–41.
[4] Masters CL, Harris JO, Gajdusek DC, Gibbs Jr CJ, Bernoulli C, Asher DM. Creutzfeldt–Jakob disease: patterns of worldwide occurrence and the significance of familial and sporadic clustering. Ann Neurol 1979;5:177–88.
[5] Zerr I, Pocchiari M, Collins S, Brandel JP, de Pedro Cuesta J, Knight RS, et al. Analysis of EEG and CSF 14–3–3 proteins as aids to the diagnosis of Creutzfeldt–Jakob disease. Neurology 2000;55:811–5.
[6] Zerr I, Bodemer M, Gefeller O, Otto M, Poser S, Wiltfang J, et al. Detection of 14–3–3 protein in the cerebrospinal fluid supports the diagnosis of Creutzfeldt–Jakob disease. Ann Neurol 1998;43:32–40.
[7] Hsich G, Kenney K, Gibbs CJ, Lee KH, Harrington MG. The 14–3–3 brain protein in cerebrospinal fluid as a marker for transmissible spongiform encephalopathies. N Engl J Med 1996;335:924–30.
[8] Aksamit Jr AJ, Preissner CM, Homburger HA. Quantitation of 14–3–3 and neuron-specific enolase proteins in CSF in Creutzfeldt–Jakob disease. Neurology 2001;57:728–30.
[9] Brandel JP, Delasnerie-Laupretre N, Laplanche JL, Hauw JJ, Alperovitch A. Diagnosis of Creutzfeldt–Jakob disease: effect of clinical criteria on incidence estimates. Neurology 2000;54:1095–9.
[10] Seno H, Tashiro H, Ishino H, Inagaki T, Nagasaki M, Morikawa S. New haplotype of familial Creutzfeldt–Jakob disease with a codon 200 mutation and a codon 219 polymorphism of the prion protein gene in a Japanese family. Acta Neuropathol (Berl) 2000;99:125–30.
[11] Hauw JJ, Sazdovitch V, Laplanche JL, Peoc'h K, Kopp N, Kemeny J, et al. Neuropathologic variants of sporadic Creutzfeldt–Jakob disease and codon 129 of PrP gene. Neurology 2000;54:1641–6.
[12] Meiner Z, Gabizon R, Prusiner SB. Familial Creutzfeldt–Jakob disease. Codon 200 prion disease in Libyan Jews. Medicine (Baltimore) 1997;76:227–37.
[13] Iwabuchi K, Endoh S, Hagimoto H, Okamoto K, Miyakawa T, Yamaguchi T, et al. Three patients from two families with familial Creutzfeldt–Jakob disease having a point mutation in the prion protein gene at codon 200 (Glu→Lys). No To Shinkei 1994;46:349–54.
[14] Kawauchi Y, Okada M, Kuroiwa Y, Ishihara O, Akai J. Familial Creutzfeldt–Jakob disease with the heterozygous point mutation at

codon 200 of the prion protein gene (Glu→Lys)–report of CJD200 brothers of Yamanashi Prefecture origin. No To Shinkei 1997;49: 460–4.
[15] Salvatore M, Pocchiari M, Cardone F, Petraroli R, D'Alessandro M, Galvez S, et al. Codon 200 mutation in a new family of Chilean origin with Creutzfeldt–Jakob disease. J Neurol Neurosurg Psychiatry 1996; 61:111–2.
[16] Chapman J, Arlazoroff A, Goldfarb LG, Cervenakova L, Neufeld MY, Werber E, et al. Fatal insomnia in a case of familial Creutzfeldt–Jakob disease with the codon 200 (Lys) mutation. Neurology 1996; 46:758–61.
[17] Antoine JC, Laplanche JL, Mosnier JF, Beaudry P, Chatelain J, Michel D. Demyelinating peripheral neuropathy with Creutzfeldt–Jakob disease and mutation at codon 200 of the prion protein gene. Neurology 1996;46:1123–7.
[18] Mendez OE, Shang J, Jungreis CA, Kaufer DI. Diffusion-weighted MRI in Creutzfeldt–Jakob disease: a better diagnostic marker than CSF protein 14–3–3? J Neuroimaging 2003;13:147–51.
[19] Bahn MM, Kido DK, Lin W, Pearlman AL. Brain magnetic resonance diffusion abnormalities in Creutzfeldt–Jakob disease. Arch Neurol 1997;54:1411–5.
[20] Bahn MM, Parchi P. Abnormal diffusion-weighted magnetic resonance images in Creutzfeldt–Jakob disease. Arch Neurol 1999;56: 577–83.
[21] Demaerel P, Baert AL, Vanopdenbosch L, Robberecht W, Dom R. Diffusion-weighted magnetic resonance imaging in Creutzfeldt–Jakob disease. Lancet 1997;349:847–8.
[22] Demaerel P, Heiner L, Robberecht W, Sciot R, Wilms G. Diffusion-weighted MRI in sporadic Creutzfeldt–Jakob disease. Neurology 1999;52:205–8.
[23] Demaerel P, Sciot R, Robberecht W, Dom R, Vandermeulen D, Maes F, et al. Accuracy of diffusion-weighted MR imaging in the diagnosis of sporadic Creutzfeldt–Jakob disease. J Neurol 2003;250:222–5.
[24] Matoba M, Tonami H, Miyaji H, Yokota H, Yamamoto I. Creutzfeldt–Jakob disease: serial changes on diffusion-weighted MRI. J Comput Assist Tomogr 2001;25:274–7.
[25] Na DL, Suh CK, Choi SH, Moon HS, Seo DW, Kim SE, et al. Diffusion-weighted magnetic resonance imaging in probable Creutzfeldt–Jakob disease: a clinical–anatomic correlation. Arch Neurol 1999;56:951–7.
[26] Nagaoka U, Kurita K, Hosoya T, Kitamoto T, Kato T. Diffusion images on brain MRI in Creutzfeldt–Jakob disease. Clin Neurol 1999;39:468–70.
[27] Schaefer PW, Grant PE, Gonzalez RG. Diffusion-weighted MR imaging of the brain. Radiology 2000;217:331–45.
[28] Yee AS, Simon JH, Anderson CA, Sze CI, Filley CM. Diffusion-weighted MRI of right-hemisphere dysfunction in Creutzfeldt–Jakob disease. Neurology 1999;52:1514–5.
[29] Nitrini R, Mendonca RA, Huang N, LeBlanc A, Livramento JA, Marie SK. Diffusion-weighted MRI in two cases of familial Creutzfeldt–Jakob disease. J Neurol Sci 2001;184:163–7.
[30] Ishida S, Sugino M, Koizumi N, Shinoda K, Ohsawa N, Ohta T, et al. Serial MRI in early Creutzfeldt–Jacob disease with a point mutation of prion protein at codon 180. Neuroradiology 1995;37:531–4.
[31] Huang N, Marie SK, Kok F, Nitrini R. Familial Creutzfeldt–Jakob disease associated with a point mutation at codon 210 of the prion protein gene. Arq Neuropsiquiatr 2001;59:932–5.
[32] Satoh A, Goto H, Satoh H, Tomita I, Seto M, Furukawa H, et al. A case of Creutzfeldt–Jakob disease with a point mutation at codon 232: correlation of MRI and neurologic findings. Neurology 1997;49: 1469–70.
[33] Shiga Y, Miyazawa K, Sato S, Fukushima R, Shibuya S, Sato Y, et al. Diffusion-weighted MRI abnormalities as an early diagnostic marker for Creutzfeldt–Jakob disease. Neurology 2004;6:443–9.
[34] Mendez OE, Shang J, Jungreis CA, Kaufer DI. Accuracy of diffusion-weighted MR imaging in the diagnosis of sporadic Creutzfeldt–Jakob disease. J Neurol 2003;250:222–5.
[35] Bergui M, Bradac GB, Rossi G, Orsi L. Extensive cortical damage in a case of Creutzfeldt–Jacob disease: clinicoradiological correlations. Neuroradiology 2003;45:304–7.
[36] Mittal S, Farmer P, Kalina P, Kingsley PB, Halperin J. Correlation of diffusion-weighted magnetic resonance imaging with neuropathology in Creutzfeldt–Jakob disease. Arch Neurol 2002;59:128–34.
[37] Cambier DM, Kantarci K, Worrell GA, Westmoreland BF, Aksamit AJ. Lateralized and focal clinical, EEG, and FLAIR MRI abnormalities in Creutzfeldt–Jakob disease. Clin Neurophysiol 2003;114: 1724–8.
[38] de Priester JA, Jansen GH, de Kruijk JR, Wilmink JT. New MRI findings in Creutzfeldt–Jakob disease: high signal in the globus pallidus on T1-weighted images. Neuroradiology 1999;41:265–8.
[39] Maeda H, Sato M, Yoshikawa A, Kimura M, Sonomura T, Terada M, et al. Brain MR imaging in patients with hepatic cirrhosis: relationship between high intensity signal in basal ganglia on T1-weighted images and elemental concentrations in brain. Neuroradiology 1997;39:546–50.

Neuropathology and Applied Neurobiology (2005), **31**, 80–87 doi: 10.1111/j.1365-2990.2004.00592.x

Fatal familial insomnia with an unusual prion protein deposition pattern: an autopsy report with an experimental transmission study

K. Sasaki*, K. Doh-ura*, Y. Wakisaka*, H. Tomoda† and T. Iwaki*

**Department of Neuropathology, Neurological Institute, Graduate School of Medical Sciences, Kyushu University, Fukuoka, and †Department of Neurology, Imazu Red Cross Hospital, Imazu, Fukuoka, Japan*

K. Sasaki, K. Doh-ura, Y. Wakisaka, H. Tomoda and T. Iwaki (2005) *Neuropathology and Applied Neurobiology* 31, 80–87

Fatal familial insomnia with an unusual prion protein deposition pattern: an autopsy report with an experimental transmission study

We recently performed a *post-mortem* examination on a Japanese patient who had a prion protein gene mutation responsible for fatal familial insomnia (FFI). The patient initially developed cerebellar ataxia, but finally demonstrated insomnia, hyperkinetic delirium, autonomic signs and myoclonus in the late stage of the illness. Histological examination revealed marked neuronal loss in the thalamus and inferior olivary nucleus; however, prion protein (PrP) deposition was not proved in these lesions by immunohistochemistry. Instead, PrP deposition and spongiform change were both conspicuous within the cerebral cortex, whereas particular PrP deposition was also observed within the cerebellar cortex. The abnormal protease-resistant PrP (PrP^{res}) molecules in the cerebral cortex of this case revealed PrP^{res} type 2 pattern and were compatible with those of FFI cases, but the transmission study demonstrated that a pathogen in this case was different from that in a case with classical FFI. By inoculation with homogenate made from the cerebral cortex, the disease was transmitted to mice, and neuropathological features that were distinguishable from those previously reported were noted. These findings indicate the possibility that a discrete pathogen was involved in the disease in this case. We suggest that not only the genotype of the PrP gene and some other as yet unknown genetic factors, but also the variation in pathogen strains might be responsible for the varying clinical and pathological features of this disease.

Keywords: Creutzfeldt-Jakob disease, NZW mouse, prion disease, thalamic form, transmissible spongiform encephalopathy

Introduction

Fatal familial insomnia (FFI) is one of the disease entities of prion disease or transmissible spongiform encephalopathy (TSE) and it is linked to a mutation at codon 178 of the prion protein gene (PRNP), aspartic acid to asparagine substitution (D178N), in conjunction with methionine at the polymorphic position 129 of the mutant allele [1]. The neuropathological hallmark of FFI is the predominance of lesions within the thalamus [2]. Clinically this disorder is characterized by progressive insomnia, dysautonomia and motor signs [3]. The D178N mutation is also associated with familial Creutzfeldt-Jakob disease (CJD). The disease phenotypes have been considered to depend on the polymorphism at codon 129 of the mutant allele, methionine (129Met) in FFI and valine (129Val) in CJD [4]. However, the FFI genotype reveals diverse clinical expression including cerebellar ataxia, dementia and autonomic abnormalities with or without insomnia [5,6]. In Japan, one FFI case [7] and some cases of the 'sporadic'

Correspondence: Kensuke Sasaki, Department of Neuropathology, Neurological Institute, Graduate School of Medical Sciences, Kyushu University, Fukuoka 812-8582, Japan. Tel: +81-92-6425539; Fax: +81-92-6425540; E-mail: ksasaki@np.med.kyushu-u.ac.jp

thalamic form of CJD [8,9] have been reported, and these have indicated a discrepancy between PRNP genotype and the disease phenotype.

We recently performed a *post-mortem* examination on a Japanese patient with a 27-month history of familial prion disease with PRNP D178N-129Met mutation. The clinical data on this patient and his family have been published in part [10]. Here we report additional clinical data and *post-mortem* neuropathological findings, as well as findings in mice infected with the patient's material.

Case report

The pedigree is presented in Figure 1. In October 1997, a 50-year-old Japanese man (Patient II-5) developed an unsteady gait, followed within a month by difficulty in speech. Although these symptoms worsened rapidly, he did not immediately develop either dementia or insomnia. He was admitted to a hospital for neurological evaluation in February 1998, and PRNP D178N-129Met mutation (heterozygous for 129Met/Val) was revealed as previously reported [10]. From October 1998, either insomnia or delirium was clearly apparent. Hyperthermia without any signs indicative of infection or inflammation, thus suggesting an autonomic sign, was also observed. He often showed reality disturbance and restlessness. He became progressively demented, developed trismus, myoclonus and horizontal nystagmus, and demonstrated increased muscle tone. Finally he became bedridden with flexion contracture. Brain computed tomography revealed mild atrophy of the cerebellum and brainstem. Electroencephalograms showed a background of 9 Hz diffuse α activities, but periodic synchronous discharges were not detected during the clinical course. Sleep activities with rapid eye movements were not recorded in sleep electroencephalograms. In January 2000, he died of pneumonia at the age of 52 years, about 27 months after the onset of disease.

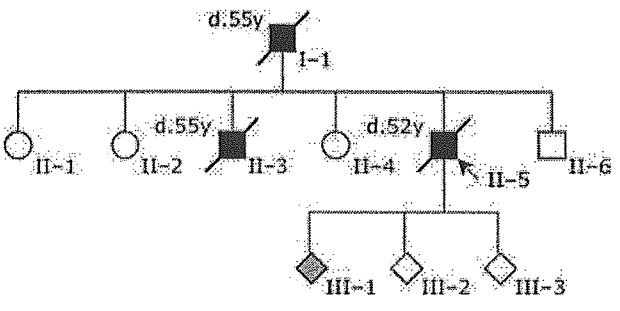

Figure 1. Family tree of the present pedigree. Patients who developed rapidly progressive cerebellar ataxia are depicted by closed symbols, along with their age at death (years old). One of the children of the present case has fatal familial insomnia genotype D178N-129Met/Met (grey symbol).

Patient II-3, one of the brothers of Patient II-5, also showed rapidly progressive cerebellar ataxia. He developed an ataxic gait, forgetfulness and dysarthria at the age of 55 years. Brain computed tomography demonstrated moderate cerebellar atrophy, and electroencephalograms showed diffuse intermittent slow activities without periodic synchronous discharges. He developed myoclonic jerks, akinetic mutism with a decorticate posture, and died 7 months after the onset. Patient I-1, the father of Patients II-5 and II-3, had also developed an ataxic gait and dementia at the age of 55 years. He died of unknown causes after a clinical course of 12 months. Neither autopsy nor PRNP analysis was carried out in either Patient I-1 or Patient II-3. One of the children of Patient II-5 was revealed to have PRNP D178N-129Met mutation (homozygous for 129Met).

Materials and methods

Autopsy was performed 6 h *post-mortem*. A frontal tip of the right cerebral hemisphere and a cerebellar tip were sampled and frozen for Western blot analysis. The remaining brain was immersion-fixed in 10% formalin for 2 weeks. Tissue blocks were immersed in 98% formic acid for 1 h and paraffin-embedded. Hematoxylin and eosin (HE) stain, Klüver-Barrera stain and Bodian's method were performed on 7-μm-thick sections. Immunohistochemical analyses were performed by a standard indirect method for glial fibrillary acidic protein (GFAP) (polyclonal, Dako, Denmark, or monoclonal, clone G-A-5, Roche, Switzerland), ferritin (polyclonal, Dako), β-amyloid precursor protein (APP) (monoclonal, clone LN27, Zymed, USA), SNAP-25 (monoclonal, clone MAB331, Chemicon, USA) and prion protein (PrP) (monoclonal, clone 3F4, Senetek, USA). For anti-PrP immunohistochemistry, sections were pretreated with hydrolytic autoclaving as previously reported [11]. Western blot analysis for protease-resistant PrP (PrP^{res}) was performed using frontal cortical and cerebellar tissue tips from this case, applying phosphotungstic acid precipitation of PrP^{res} as described previously [12] with 50 μg/ml proteinase K (PK) digestion, along with a control case with sporadic

CJD (77-year-old man, duration of illness was 9 months, 129Met/Met). Transmission study was performed as described previously [13]. Briefly, frontal cortical tissue tips were aseptically homogenized with nine volumes of saline, and after removal of debris by low-speed centrifugation the supernatant was used as 10% homogenate. Twenty microliters of 10% homogenate were injected intracerebrally into female NZW mice or female Tg7 mice expressing hamster PrP but not endogenous murine PrP. Sections of infected mice were analysed by HE stain and also by immunohistochemistry for PrP (polyclonal, PrP-C, IBL, Japan) and GFAP (clone G-A-5, Roche). Permission for the animal experiments was obtained from the Animal Experiment Committee of Kyushu University.

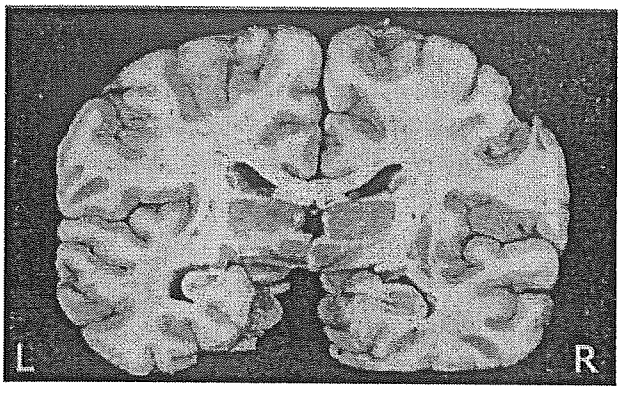

Figure 2. Coronal section at the thalamic level. The medial part of the thalamus is atrophic and the third ventricle is dilated.

Results

The brain weighed 1350 g before fixation. The cerebellum showed slight atrophy, whereas the volume of the forebrain was preserved. Coronal sections showed atrophy of the medial part of the thalamus and symmetrical dilatation of the third ventricle (Figure 2).

The summary of histological examination is shown in Figure 3. Marked neuronal loss and moderate astrogliosis in the thalamus were observed, most prominently in its centromedial nucleus and dorsomedial nucleus. However, spongiform change was imperceptible (Figure 4A,B). Neuronal loss and gliosis in the medial portion of the inferior olivary nucleus were also apparent (Figure 4C,D). In the cerebellum there was mild loss of granular cells, and the molecular layer was slightly atrophic. There were localized lesions of spongiosis in the cerebellar molecular layer. Purkinje's cells appeared not to be decreased in number, but they often demonstrated shrunken features. The cerebellar white matter showed diffuse myelin pallor. The cerebral cortex showed uneven distribution of spongiform change and neuronal loss (Figure 4E). There was no apparent difference in the intensities of the cortical lesions among the lobes of the cerebrum except that the lesions are more prominent in the entorhinal cortex and less in the occipital lobe. Moderate astrogliosis was associated with the spongiform lesions (Figure 4F).

Immunohistochemistry for PrP revealed that there was no punctate or plaque-type immunoreactivity in the thal-

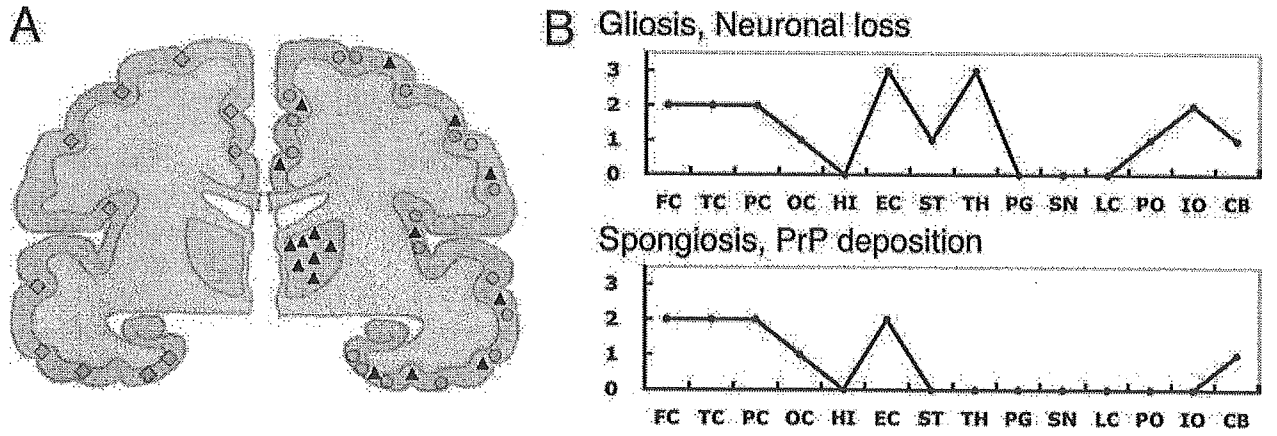

Figure 3. Lesion profiles of the present case. A: schematic drawing of the distribution of prion protein (PrP) deposition (diamonds), spongiosis (circles) and neuronal loss (triangles) in this case, which can be compared to that of fatal familial insomnia (FFI) and 178CJD shown in ref. [19]. B: lesion profiles in respect to gliosis/neuronal loss and spongiosis/PrP deposition. Brain regions studied were: frontal cortex (FC), temporal cortex (TC), parietal cortex (PC), occipital lobe (OC), hippocampus (HI), entorhinal cortex (EC), striatum (ST), thalamus (TH), substantia nigra (SN), periaqueductal grey (PG), pons (PO), locus ceruleus (LC), medulla oblongata (ME), cerebellum (CB). The vertical axis is the degree of lesion graded as follows. 0: not detectable; 1: mild; 2: moderate; 3: severe.